Insights into the Base Catalysis Exerted by the DD-Transpeptidase from *Streptomyces* K15: A Molecular Dynamics Study†

Natalia Díaz, Tomás L. Sordo, and Dimas Suárez*

Departamento de Química Física y Analítica, Universidad de Oviedo, C/ Julián Clavería, 8. 33006, Oviedo (Asturias), Spain

Received August 20, 2004; Revised Manuscript Received December 9, 2004

ABSTRACT: Herein, we present results from molecular dynamics simulations of the DD-transpeptidase/penicillin-binding protein from *Streptomyces* K15 and its Michaelis complex with benzylpenicillin. For the apo-enzyme, six different configurations of the active site were modeled in aqueous solution and their relative stabilities were estimated by means of quantum mechanical energy calculations. The energetically most stable configuration has a neutral Lys_{213} residue. In this configuration, the nucleophilic Ser_{35} hydroxyl group interchanges with a water molecule in the "oxy-anion hole" and the Lys_{38}/Lys_{213} ammonium/amino groups are connected through the Ser_{96} hydroxyl group. Subsequently, the enzyme−penicillin complexes corresponding to the four most stable configurations of the apo-enzyme were modeled. In the presence of the β-lactam antibiotic, the configuration with a neutral Lys_{38} residue is favored energetically and shows the best orientation for nucleophilic attack. In addition, a very stable contact between the Ser_{35} hydroxyl group and the neutral amino group of Lys_{38} supports the assignation of Lys_{38} as the base catalyst for the acylation step. Finally, some mechanistic implications of enzyme−inhibitor contacts involving the benzylpenicillin carboxylate group are also discussed.

β-Lactam antibiotics such as penicillins and cephalosporins exert their lethal action by inhibiting a family of bacterial enzymes termed the penicillin-binding proteins (PBPs)[1] (*1*). These enzymes are involved in the synthesis and remodeling of the peptidoglycan, which is the main macromolecular component of the bacterial cell wall. The peptidoglycan is formed by linear strands of glycan consisting of alternating *N*-acetylglucosamine and *N*-acetylmuramic acid residues, and short peptide chains characterized by a C-terminal D-Ala−D-Ala sequence. The PBPs are classified as DD-carboxypeptidases if they catalyze the cleavage of the D-Ala−D-Ala fragment by forming a transient acyl-enzyme intermediate that is subsequently hydrolyzed by a water molecule, or as DD-transpeptidases if the acyl-enzyme intermediate reacts with a terminal amino group from another peptide chain to form a cross-link. The transpeptidase activity of PBPs results in a tight weblike structure, which is crucial to maintain the rigidity of the cell wall and the viability of the bacteria, whereas the carboxypeptidase action seems to modulate the degree of the cross-linking. The PBP enzymes also form acyl-enzyme intermediates with penicillins and other β-lactam antibiotics, as a result of the structural similarity between the β-lactam nucleus and the D-Ala−D-Ala fragment of the peptidoglycan (*2*). However, the β-lactam−PBP covalent complex is quite stable resulting thus in the prolonged inhibition of the bacterial enzyme and the antibiotic activity observed (*3*).

The efficiency of β-lactam antibiotics is continuously challenged by the emergence of resistant bacterial strains, which employ two major strategies to escape the lethal action of antibiotics (*4*). On one hand, bacteria are capable of modifying their PBPs to reduce their sensitivity to antibiotics while maintaining a similar degree of activity toward their peptide substrates. On the other hand, they synthesize enzymes called β-lactamases that efficiently hydrolyze the acyl-enzyme intermediate formed with β-lactams. β-Lactamases are the primary cause of resistance to β-lactam antibiotics, and some of them can be considered as perfect enzymes because the rate of reaction with their best substrates is nearly diffusion limited (*5*).

Bacteria possess a number of different PBPs that can be divided into two groups, the low molecular weight (LMW) and the high molecular weight (HMW) enzymes (*3*). The LMW PBPs contain a single transpeptidase/hydrolase domain, whereas the HMW PBPs can be further divided into monofunctional transpeptidase enzymes and bifunctional enzymes with transpeptidase and glycosyltransferase domains. β-Lactamases are soluble, monofunctional enzymes composed of a single domain similar to the DD-peptidase domain of the PBPs. Traditionally, they are classified into four groups according to their sequence homology. The β-lactamases of the classes A, C, and D are serine-enzymes like most of the PBPs, whereas the zinc-metallo-enzymes are grouped together in class B (*6*).

PBPs and β-lactamases are considered to be evolutionary related (*7*). Thus, the peptidase module of PBPs and all β-lactamases share a common fold characterized by a two-domain structure: a mainly helical domain and an α/β

† This research was supported in part by the Spanish Ministry of Science and Technology via Grant SAF2001-3526, and by the FICyT (Asturias, Spain) via contract DOC02-14 to N.D.

* To whom correspondence should be addressed. Phone: +34-985182266. FAX: +34-985103125. E-mail: dimas@uniovi.es.

[1] Abbreviations: BP, benzylpenicillin; D&C, divide and conquer; DFT, density functional theory; MD, molecular dynamics; QM, quantum mechanical; QM/MM, hybrid quantum mechanical and molecular mechanical; PB, Poisson−Boltzmann; PBPs, penicillin-binding proteins; PDB, Protein Data Bank; PES, potential energy surface.

10.1021/bi048193g CCC: $30.25
Published on Web 02/08/2005

domain. For the serine enzymes, the active site is found at the interface of these two domains and displays a remarkable conservation of the spatial arrangement of three conserved motifs (*8*). The first motif is located at the amino terminus of a long helix and contains the nucleophilic serine and an absolutely conserved lysine (SXXK). The second motif, S(Y)XN(C), is found in a loop and positions an essential hydroxyl group from a serine or a tyrosine side chain in the active site. The third motif, K(H)S(T)G, which contributes to the so-called "oxyanion hole" that interacts with the reactive amide carbonyl group, is situated on the innermost β3 strand of the β-sheet and is considered to play a role in orienting the incoming substrate or inhibitor. In addition to these three conserved motifs, class A β-lactamases present a fourth relevant element, DXXN, which is part of an Ω loop (*9*).

The catalytic role of the active site residues common to all PBPs and β-lactamases is not completely understood. Different residues of the conserved motifs have been proposed to be the crucial base catalyst that is required to activate the nucleophilic serine during acylation. For the best characterized enzymes, the class A β-lactamases, several lines of evidence support a central role for the glutamic acid of the DXXN motif (Glu_{166}) as the base catalyst along the reactive pathway (*10*−*15*). In the class C β-lactamases and some PBPs such as the DD-carboxypeptidase from *Streptomyces* R61, it has been proposed that the lysine residue in the first motif or the tyrosine residue present in the second conserved motif could act as the general base catalyst (*16*−*21*). The enzymatic activity of the class D β-lactamases has been related to the carbonatation of the invariant lysine residue present in the SXXK motif, which in turn should possess an abnormally low pK_a value (*22*). Concerning the PBPs, different crystallographic, mutagenesis, and kinetic experiments point toward the lysine residue of the first conserved motif as the base catalyst (*23*−*25*).

The previous proposals are not conclusive regarding the identity of the base catalyst and/or the protonation configuration of the PBPs. In this work, we theoretically investigate the native form of the DD-transpeptidase from *Streptomyces* K15 (hereafter referred to as the K15 enzyme) and its complex with benzylpenicillin. The K15 enzyme is a 262-amino acid LMW PBP with a strict transpeptidase activity. The second-order rate constant for enzyme acylation by benzylpenicillin (150 M^{-1} s^{-1}) characterizes the K15 enzyme as a PBP of intermediate penicillin sensitivity (*26*). Structurally, the enzyme displays a remarkable degree of homology with class A β-lactamases and with the DD-peptidase domain of other PBPs, like PBP5 from *Escherichia coli* (*27*). The active site is defined by the previously described three conserved structural elements (Ser_{35}−Thr_{36}−Thr_{37}−Lys_{38}, Ser_{96}−Gly_{97}−Cys_{98}, and Lys_{213}−Thr_{214}−Gly_{215}). Among the residues that build up these conserved motifs, Lys_{38} and Ser_{96} seem to be crucial for catalysis. The Lys_{38} → His and Ser_{96} → Ala mutations almost completely abolish penicillin binding and severely impair the transpeptidase activity (*25*). Another important residue, Cys_{98}, is present in the second motif instead of the usual asparagine residue observed in other enzymes. The low value of the Cys_{98}−Sγ···Nζ−Lys_{38} distance in the X-ray structure (2.7 Å, a value similar to that of the Asn@Oδ2···Nζ@Lys contact observed in other PBPs and β-lactamases) suggests that two different structures

Scheme 1

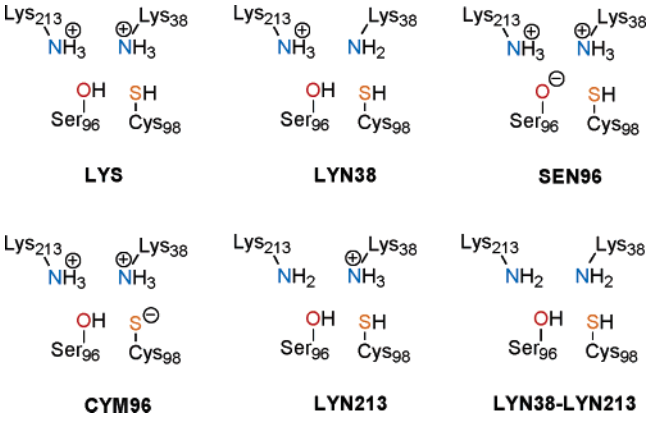

would be possible: (a) Lys_{38} could be deprotonated, in which case a Cys_{98}−SH···:N$_\zeta$H$_2$−Lys_{38} hydrogen bond should be present in the X-ray structure; (b) the thiol group of Cys_{98} could be negatively charged forming thus a Cys_{98}−Sγ^-···$^+$N$_\zeta$H$_3$−Lys_{38} salt bridge interaction. Nonetheless, the presence of an anionic cysteine residue seems unlikely on the basis of mutagenesis experiments. Thus, the Cys98Asn mutation in the K15 enzyme increases k_{cat}/K_M for its acylation reaction with cephalosporins, hardly changes the k_{cat}/K_M value for benzylpenicillin, and decreases the catalytic efficiency with peptide substrates (*25*).

Concerning the catalytic mechanism of the K15 enzyme, Rhazi et al. have proposed that Lys_{38} acts as the base catalyst during nucleophilic attack, and that Ser_{96} is a key residue for assisting the proton transfer to the substrate/inhibitor leaving amino group (*25*). However, this mechanistic proposal contrasts with former theoretical pK_a calculations that assign a pK_a value of 14.0 to Lys_{38} either in the apo-enzyme or in a modeled Michaelis complex with cefoxitin (*28*). The same calculations attribute a significant low pK_a value to Lys_{213} (7.4 in the apo-enzyme and 9.3 in the complex) and to Cys_{98} (7.2 in the apo-enzyme and 8.1 in the complex). From these results, it is conceivable that Lys_{213} and Cys_{98} could be deprotonated in the native form of the K15 enzyme. Hence, it seems that the theoretical and experimental observations on the PBP enzyme from *Streptomyces* K15 are somewhat contradictory.

Clearly, to increase our understanding of the reaction mechanism of the K15 DD-transpeptidase it is necessary to find out which are the actual protonation configurations of the active site residues relevant to catalysis. To fulfill this goal, we decided to perform an analysis of the protonation configurations of the K15 active site that could be important according to X-ray analyses, theoretical pK_a calculations, and experimental kinetic results. Namely, we selected six configurations of the fully solvated enzyme differing in the protonation state of the Lys_{38}, Ser_{96}, Cys_{98}, and Lys_{213} residues (see Scheme 1) and examined them by means of extended molecular dynamics (MD) simulations and quantum mechanical (QM) calculations. Along the simulations, we characterized the interactions between the important functional groups, and the structural and dynamical changes related to protonation/deprotonation of the active site residues. The free energy of each configuration was estimated by using semiempirical quantum chemical methodologies to compute enthalpies and solvation energies for protein

subsystems, while molecular mechanics normal mode calculations were used to account for entropic effects (the use of the semiempirical methodologies was validated by performing density functional theory (DFT) calculations on cluster models involving the Lys_{38}, Ser_{96}, Cys_{98}, and Lys_{213} side chains). Subsequently, the complexed form of the K15 enzyme with benzylpenicillin (BP) was simulated for the four configurations of the apo-enzyme that resulted to be more favorable energetically. In this way, we characterized the structural and dynamical changes upon inhibitor binding as well as the specific role of key residues in anchoring the ligand. Binding energies for the four complexes were also estimated. Finally, we discuss the ability of our results to help solve the discrepancies between experimental and theoretical results on the K15 enzyme, and suggest a plausible catalytic mechanism for this transpeptidase enzyme.

METHODS

MD Simulations of the Unbound Form of the K15 Enzyme. Initial coordinates for the protein atoms and the crystallographic water molecules were taken from the solid-state structure of the K15 enzyme at 2.0 Å (PDB code 1SKF) (*27*). The ionizable residues were set to their normal ionization states at pH 7, except Lys_{38}, Ser_{96}, Cys_{98}, and Lys_{213} that were ionized according to Scheme 1 in the six trajectories examined for the apo-enzyme. His_{76} and His_{135} were protonated at Nδ, whereas His_{138} was protonated at Nϵ in agreement with previous electrostatic calculations (*28*). The protein atoms, as well as all the water molecules of the crystal structure, were surrounded by a periodic box of TIP3P (*29*) water molecules that extended 10 Å from the protein atoms. Cl^- counterions were placed by the LEaP program (*30*) to neutralize the system. This resulted in a total of ~3897 protein atoms being solvated by 149 X-ray water molecules and 11 317 additional water molecules.

The parm94 version of the all-atom AMBER force field was used to model the system (*31*). The solvent molecules and counterions were initially relaxed by means of energy minimizations and 50 ps of MD. Then the full system was minimized to remove bad contacts in the initial geometry. All the MD simulations were carried out using SANDER included in version 7.0 of the AMBER suite of programs (*32*). The time step was chosen to be 1.5 fs and the SHAKE algorithm was used to constrain all bonds involving hydrogen atoms. A nonbonded cutoff of 10.0 Å was used and the nonbonded pairlist was updated every 25 time steps. The pressure (1 atm) and the temperature (300 K) of the system were controlled during the MD simulation by Berendsen's method (*33*). Periodic boundary conditions were applied to simulate a continuous system. To include the contributions of long-range interactions, the Particle-Mesh-Ewald (PME) method (*34*) was used with a grid spacing of ~1 Å combined with a fourth-order B-spline interpolation to compute the potential and forces in between grid points.

For all the examined configurations, an equilibration period of 200 ps resulted in stable trajectories as evidenced by the convergence of the dimensions of the simulation box and the evolution of the total energy of the system. Subsequently, 2.0 ns trajectories were computed and coordinates were saved for analysis every 100 time steps. All of the MD results were analyzed using the CARNAL module of AMBER 7.0 and some other specific trajectory analysis software developed locally. Structural figures were produced with the programs Molscript (*35*) and Raster3D (*36*).

MD Simulations of the Michaelis Complex Formed between the K15 Enzyme and Benzylpenicillin. The LYS, LYN38, SEN96, and LYN213 configurations were also modeled in the presence of a benzylpenicillin molecule bound to the active site (LYS−BP, LYN38−BP, SEN96−BP, and LYN213−BP models). In the X-ray structure of the apo-enzyme, the nucleophilic serine hydroxyl group (Ser_{35}) is located in the "oxy-anion hole" formed by the backbone amino groups of Ser_{35} and Ser_{216}, impeding thus the access of the β-lactam carbonyl group to the "oxy-anion hole". Hence, we manually performed a rotation of the Ser_{35} side chain followed by energy-minimization of the apo-enzyme in its LYN213 configuration and a short MD simulation (50 ps) with a constraint on the Ser_{35}−Oγ···N−Ser_{216} distance. From this relaxed LYN213 configuration, several K15−benzylpenicillin complexes with reasonably good enzyme−inhibitor contacts were obtained with the AUTODOCK program (*37*, *38*). From these, we selected a low-energy complex in which the Ser_{35}−Oγ···C7−BP distance was 3.4 Å, which was further relaxed through a short MD simulation with harmonic constraints on the Ser_{35}−N···O8−BP (3.00 Å), Ser_{216}−N···O8−BP (2.80 Å), and Ser_{35}−Oγ···C7−BP (3.10 Å) distances to fully accommodate the β-lactam carbonyl group within the K15 "oxy-anion hole". The resulting structure was employed as the starting point for the four K15−BP trajectories following simulation protocols identical to those used for the unbound models. For the BP inhibitor, we employed the AMBER parameters that have been described in a previous work (*10*, *39*).

QM Calculations on Small Cluster Models. We explored the potential energy surface (PES) in aqueous solution of cluster systems relevant to the K15 active site configurations using DFT methodologies (*40*). Our cluster model included the Lys_{38}, Cys_{98}, Lys_{213} side chains, and the Ser_{96} residue, which are interconnected through a network of hydrogen bonds in the active site. The initial coordinates for the cluster atoms were extracted from the previously edited 1SKF crystal structure. Once the cluster model of each PBP configuration was constructed, we located its corresponding minimum on the aqueous solution PES at the B3LYP/6-31G* and B3LYP/6-31+G** levels of theory using the Jaguar program (*41*). During geometry optimizations, the Cβ atom of the Lys_{38}, Cys_{98}, and Lys_{213} side chains, and the backbone N and O atoms of Ser_{96} were fixed at their initial positions to maintain the relative orientation of the cluster residues found in the X-ray structure. Solvent effects were taken into account by means of the Poisson−Boltzmann (PB) solver (*42*) included in Jaguar assuming a value of 80 for the dielectric constant of the surrounding continuum. To characterize the critical points, we carried out numerical frequency calculations at the B3LYP/6-31G* level. The free energy in aqueous solution for the cluster models was estimated by adding solvation energies to the electronic energies complemented by thermal corrections to enthalpy as evaluated with the B3LYP/6-31G* frequencies.

The free energy of the cluster models in solution was recomputed at the semiempirical PM3 level (*43*) using the DivCon program (*41*), which includes a PB solver (*44*) similar to that found in the Jaguar program. Since geometry

optimization in solution is not implemented in DivCon, the cluster models were first relaxed via QM/MM energy minimizations. Thus, the cluster atoms were surrounded by a 25 Å solvent cap of TIP3P water molecules centered at the Oγ atom of the Ser_{96} fragment. After having equilibrated the solvent cap through a 50 ps MD run, each cluster model was subject to QM/MM energy minimization using the ROAR 2.0 program (*45*) (the PM3 Hamiltonian was used to describe the cluster atoms and the TIP3P force field was used for the water molecules). After geometry optimization, coordinates of the water molecules were removed and energies of the cluster models were recomputed by performing single point PM3 calculations in solution using DivCon.

The DFT structures and their free energies in solution were compared with those obtained from the PM3 calculations to test the ability of the semiempirical method to reproduce the energies and structures of the cluster models. In addition, a "high level correction" factor was derived for some cluster models by taking into account the difference between its DFT and PM3 free energies ($G_{DFT} - G_{PM3}$). This energetic term can be added a posteriori to refine the average semiempirical free energies of the K15 configurations in the solvated protein (see below).

Energetic Analyses of the MD Trajectories. The so-called molecular mechanics Poisson−Boltzmann surface area (MM-PBSA) approach is applied to perform many classes of $\Delta G_{binding}$ calculations (enzyme−ligand, protein−protein, DNA−protein) (*46*−*48*). Basically, MM-PBSA calculations predict mean values of interaction free energies as estimated over a series of representative (∼50−100) snapshots extracted from classical MD simulations. Herein, we employed a variant of the MM-PBSA approach by carrying out semiempirical QM calculations to estimate the free energies of the different protein configurations (QM-PBSA calculations). Thus, the average free energy of the protein systems was estimated according to the following equation:

$$\bar{G} \approx \bar{H}_{QM} + \Delta\bar{G}_{solv} - T\bar{S}_{MM} \quad (1)$$

where $\bar{G}$ is the calculated average free energy, $\bar{H}_{QM}$is the average QM heat of formation of the solute that accounts for intraprotein and enzyme−ligand effects, $\Delta\bar{G}_{solv}$ is the average solvation energy, which can be calculated preferably using a QM Hamiltonian coupled with a continuum model, and $-T\bar{S}_{MM}$ is the solute entropy, which can be estimated by molecular mechanics normal mode calculations.

In this work, a set of 50 representative structures extracted every 40 ps along the MD trajectories were postprocessed to calculate the average free energy for the simulated K15 configurations. Prior to the QM-PBSA calculations, the selected set of snapshots for each configuration were subject to QM/MM energy minimization. For the apo-enzyme, the QM region in the QM/MM calculations comprised the Ser_{35}, Ser_{96}, Asp_{143}, Thr_{214} residues, and the side chains of Lys_{38}, Cys_{98}, and Lys_{213}. For the benzylpenicillin-complexed structures, the QM region included the BP inhibitor, the Ser_{35} and Ser_{216} residues, and the side chain of Lys_{38}, Ser_{96}, Lys_{213}, Thr_{214}, and Arg_{248}. Atoms in the QM region were allowed to move during the QM/MM minimizations, while the rest of the protein and a solvent cap of 1500 water molecules centered on the Oγ@Ser_{35} atom (MM region) were held fixed. The PM3 Hamiltonian was used to describe the QM region and the AMBER force field was used for the rest of the system. Hydrogen link atoms were placed at the corresponding atoms to cap exposed valence sites due to bonds which crossed the QM-MM boundary. The ROAR 2.0 program (*45*) was used to carry out the QM/MM minimizations. From the QM/MM relaxed structures, we selected protein subsystems (∼1000 atoms) that were composed of all residues within a distance of ∼12 Å to Oγ@Ser_{35} (residues: Gly_{34}−Leu_{46}, Asn_{70}−Ala_{75}, Leu_{94}−Tyr_{102}, Asp_{140}−Ala_{149}, Lys_{197}−Asn_{200}, Val_{212}−Val_{225}, Ile_{245}−Ala_{252}). Terminal *N*-methylamine or acetyl groups were placed at the C and N backbone atoms of those residues cut out from the protein main chain by the truncation process. In addition, the BP inhibitor was also extracted in the case of the K15−BP complexes.

In practice, semiempirical QM calculations on large systems can be done efficiently by using linear scaling self-consistent-field techniques (*49*). Hence, we performed single-point PM3 calculations on the subsystems using the divide and conquer (D&C) approach (*50*, *51*). We preferred PM3 to AM1 owing to its better performance for hydrogen-bond contacts (*52*) and its lower mean absolute error in the prediction of heats of formation for organic molecules. Incorporation of solvent effects within the QM methodology was accomplished by merging the D&C algorithm with the PB equation (*44*). In these QM-PB calculations, the solute was represented by Charge Model 2 (CM2) atomic charges (*53*). The set of DREIDING atomic radii was used in the QM-PB calculations (*54*). An additional "nonpolar" contribution due to the creation of a solute cavity in the continuum is accounted for by a term proportional to the solvent accessible surface area of the solute as in the MM-PBSA approach. The DivCon program (*55*) was employed to perform the D&C semiempirical calculations using the dual buffer layer scheme (inner buffer layer of 4.0 Å and an outer buffer layer of 2.0 Å) with one protein residue per core. This D&C *subsetting* with a total buffer region of 6.0 Å gives accurate relative energies (*56*). A cutoff of 9.0 Å was used for the off-diagonal elements of the Fock, one-electron, and density matrices.

Solute entropic contributions were estimated for the series of subsystems with ∼1000 atoms by using the *nmode* module of the AMBER 7.0 package. This program uses the normal modes and standard statistical thermodynamical formulas to estimate entropic contributions. Prior to the normal mode calculations, the geometries of the subsystems described by their AMBER representations were minimized until the root-mean-square deviation of the elements in the gradient vector was less than 10^{-5} kcal/(mol Å). The ROAR 2.0 program was used to carry out the geometry optimizations driven by a limited memory BFGS minimizer (*57*). All minimizations and normal mode calculations were carried out with a distance-dependent dielectric constant ($\epsilon = 4r$) to mimic solvent screening and with no cutoff for nonbonded interactions. As noted in previous work (*58*), this normal-mode analysis determines only approximate estimates of the solute entropy.

For the configurations representing the K15 enzyme complexed with benzylpenicillin, we estimated the ΔG for ligand binding to the protein using the following equation:

$$\Delta G = \bar{G}_{complex} - \bar{G}_{protein} - \bar{G}_{substrate} \quad (2)$$

where the three *G* terms were evaluated using the snapshots from a single MD trajectory of the complex (the one trajectory approximation). For the $\Delta G_{binding}$ calculations, we also took into account the dispersive nonpolar interactions that are not considered in the semiempirical QM calculations by adding the attractive part of the AMBER Lennard-Jones potential (*59*) to the eq 1 in the following manner:

$$\bar{G} \approx \bar{H}_{QM} + \frac{LJ}{R^6} + \Delta\bar{G}_{solv} - T\bar{S}_{MM} \quad (3)$$

Binding free energies were computed for a standard state of 1 M. As a consequence, the translational entropy for each component (*complex, protein, ligand)* is 6.4 cal mol^{-1} K^{-1} smaller than the entropy value obtained for the standard state of an ideal gas owing to the change in concentration from 0.045 M (ideal gas) to 1 M (solution) (*48*).

RESULTS

RMSD Values and RMS Flexibility for the Apo-Enzyme. In Table S1 of the Supporting Information, the heavy atom root-mean-square deviations (RMSD) of the K15 PBP relative to its initial crystal structure are given for the most relevant structural elements, including the three conserved structural motifs that define the active site (helix α2, α4/α5 loop, and strand *β*3). Data in this table show that the structural changes in the protein taking place during the course of the MD simulations were not large. In addition, the all-atom RMSD values are comparable for the different trajectories (1.1−1.3 Å), that is, the global structure of the enzyme is not significantly affected by the protonation state of Lys_{38}, Ser_{96}, Cys_{98}, and Lys_{213}. The RMS flexibility, calculated by comparing the instantaneous protein structure to the average one, is also similar for the different trajectories (∼0.8−1.1 Å). For the active site, the RMSD and RMSF values across the six trajectories are quite similar, showing that the structure and flexibility of the active site region are only moderately influenced by the ionization state of the selected residues.

Structure of the Active Site. In the X-ray structure, the K15 active site is characterized by a dense hydrogen-bonding network that interconnects the catalytically relevant residues (Ser_{35}, Lys_{38}, Ser_{96}, Cys_{98}, Lys_{213}, Ser_{216}, etc.) and some solvent molecules. Thus, the hydroxyl group of the nucleophilic serine (Ser_{35}) is located in the "oxy-anion hole" formed by the backbone NH groups of Ser_{35} and Ser_{216} (O*γ*···N distance of 2.9 and 3.1 Å, respectively). The lysine residue of the first conserved motif (Lys_{38}) strongly interacts with the Cys_{98} side chain (Lys_{38}−Nζ···S*γ*−Cys_{98} = 2.7 Å), while Ser_{96} is hydrogen bonded to both Lys_{38} and Lys_{213} with O*γ*···Nζ distances of 2.9 Å. Lys_{213} also interacts with the backbone carbonyl group of Thr_{214} (Lys_{213}−Nζ···O−Thr_{214} = 3.1 Å) and with Met_{93} through a water molecule. Another active site residue (not conserved in all PBPs) is Arg_{248}, whose side chain interacts with Gly_{215} in the X-ray structure (Arg_{248}−N*η*2···O-Gly_{215} = 2.6 Å; a similar contact is observed in class A *β*-lactamases).In principle, the comparison of the interresidue contacts observed along the MD simulations with those present in the initial X-ray structure could help identify the most probable configuration of the K15 active site given that the hydrogen-bonding network at the active site is intimately related to the protonation state of the active site residues. Figure 1 shows representative snapshots extracted from the six MD simulations as well as schematic representations of the most stable hydrogen-bond contacts including their percentages of occurrence and their average distances. In Table S2 of the Supporting Information we collect the average values for the most significant active site interatomic distances.

Concerning the nucleophilic serine residue, five of the six trajectories maintain the Ser_{35} side chain within the "oxy-anion hole" formed by the backbone amino groups of Ser_{35} and Ser_{216}. In contrast, the Ser_{35}−O*γ*···HN−Ser_{216} contact is practically lost along the LYN213 trajectory. In this enzyme configuration, the nucleophilic serine, which enters/leaves the "oxy-anion hole" exchanging with bulk water molecules, exhibits a significant side chain flexibility.

In our simulations, the distance between Lys_{38}@Nζ in the first conserved motif and the Cys_{98} side chain is significantly longer than that in the initial solid-state structure. The closest Lys_{38}···Cys_{98} contact (3.02 ± 0.11 Å) is observed when both residues are charged forming a Cys_{98}−S^-···^+H_3N−Lys_{38} salt bridge (CYM98). On the other hand, a novel NζH···O═C interaction, not present in the initial X-ray structure, connects the Lys_{38} side chain with the backbone carbonyl group of Asp_{143} in all the trajectories excepting the SEN96 one (see Figure 1). In addition, the Lys_{38} ammonium group is able to interact directly with the Asp_{143} carboxylate group along the LYS simulation: 57% of abundance with an average distance of 2.78 ± 0.12 Å.

The Lys_{38}···Ser_{96}···Lys_{213} association found in the X-ray structure is perfectly stable along the SEN96 trajectory thanks to strong ionic contacts between the anionic serine and the ammonium groups of Lys_{38} and Lys_{213}. When the anionic Ser_{96} and one of the ammonium groups are neutralized, the Lys_{38}···Ser_{96}···Lys_{213} association is also stable as observed in the LYN38 and the LYN213 MD simulations, which present large occupancies for the corresponding Lys_{38}···Ser_{96} and Ser_{96}···Lys_{213} hydrogen bonds: 69−100% for LYN38 and 95−73% for LYN213. The hydrogen-bond sequence in these contacts along the LYN38 and LYN213 trajectories is suitable for proton transfer to occur from the protonated ammonium side chain to the amino group of the neutral lysine.

Lys_{213} interacts with water molecules in all the simulations (0.8−1.8 water molecules as estimated by integration of the first peak of the atomic radial distribution function of water molecules around Nζ@Lys_{213}). In three of the configurations examined (LYS, LYN38, CYM98), one water molecule connects the lysine side chain with the carbonyl group of Met_{93} forming a stable water bridge (occupancy of 66−82%) in agreement with the initial solid-state structure. However, a direct Lys_{213}−Nζ···O-Met_{93} interaction is formed for the rest of trajectories. On the other hand, the stability of the contact between Lys_{213} and the backbone carbonyl group of Thr_{214} varies with the six trajectories of the apo-enzyme (see Figure 1).

The interaction between the backbone carbonyl group of Gly_{215} and the side chain of Arg_{248} is stable only for the SEN96, CYM98, and LYN38_LYN213 configurations. In the other models, the Arg_{248} side chain is displaced by a water molecule which locates between the Arg_{248} guanidinium and the Gly_{215} carbonyl groups.

a) X-ray

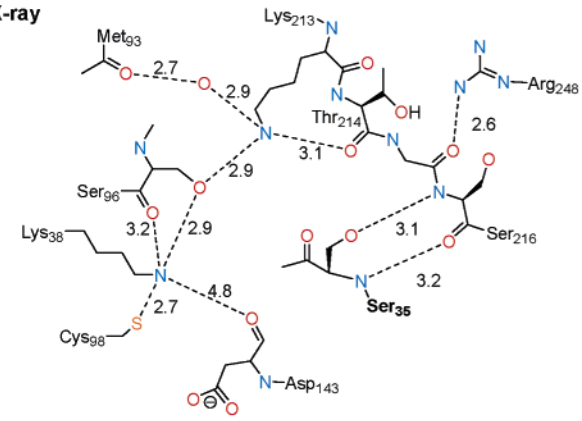

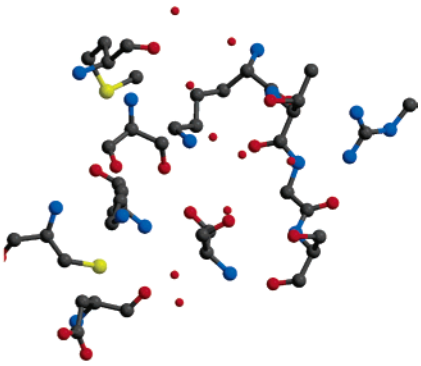

b) LYS

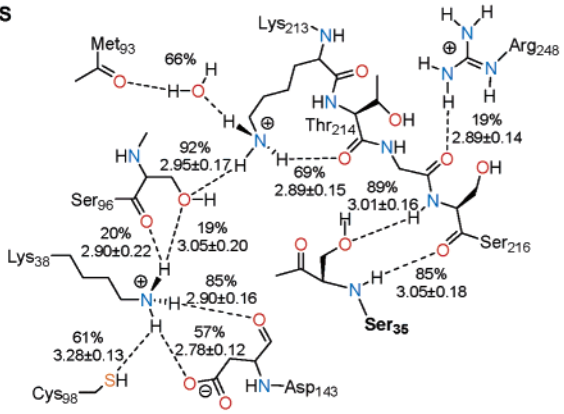

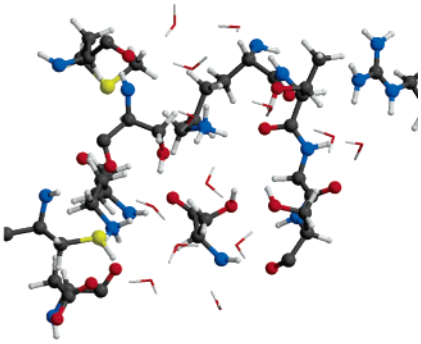

c) LYN38

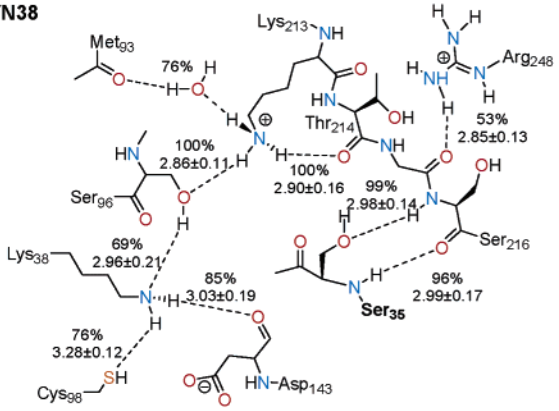

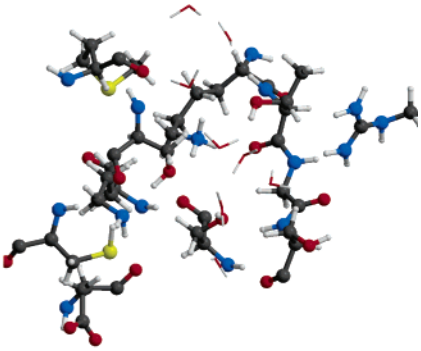

d) SEN96

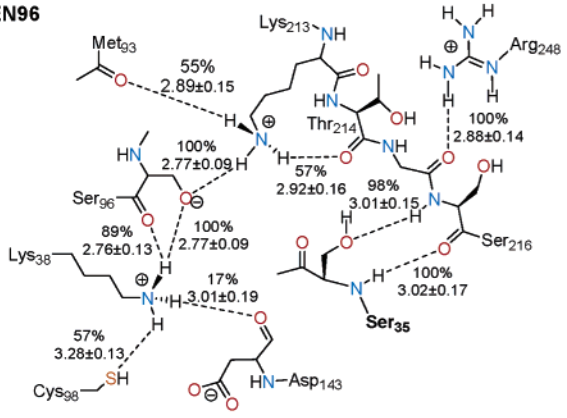

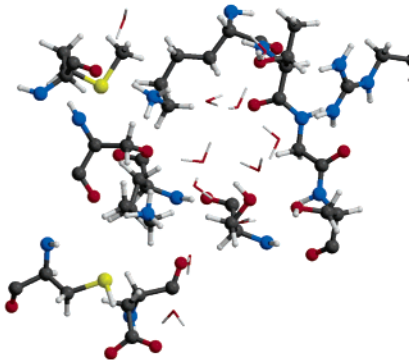

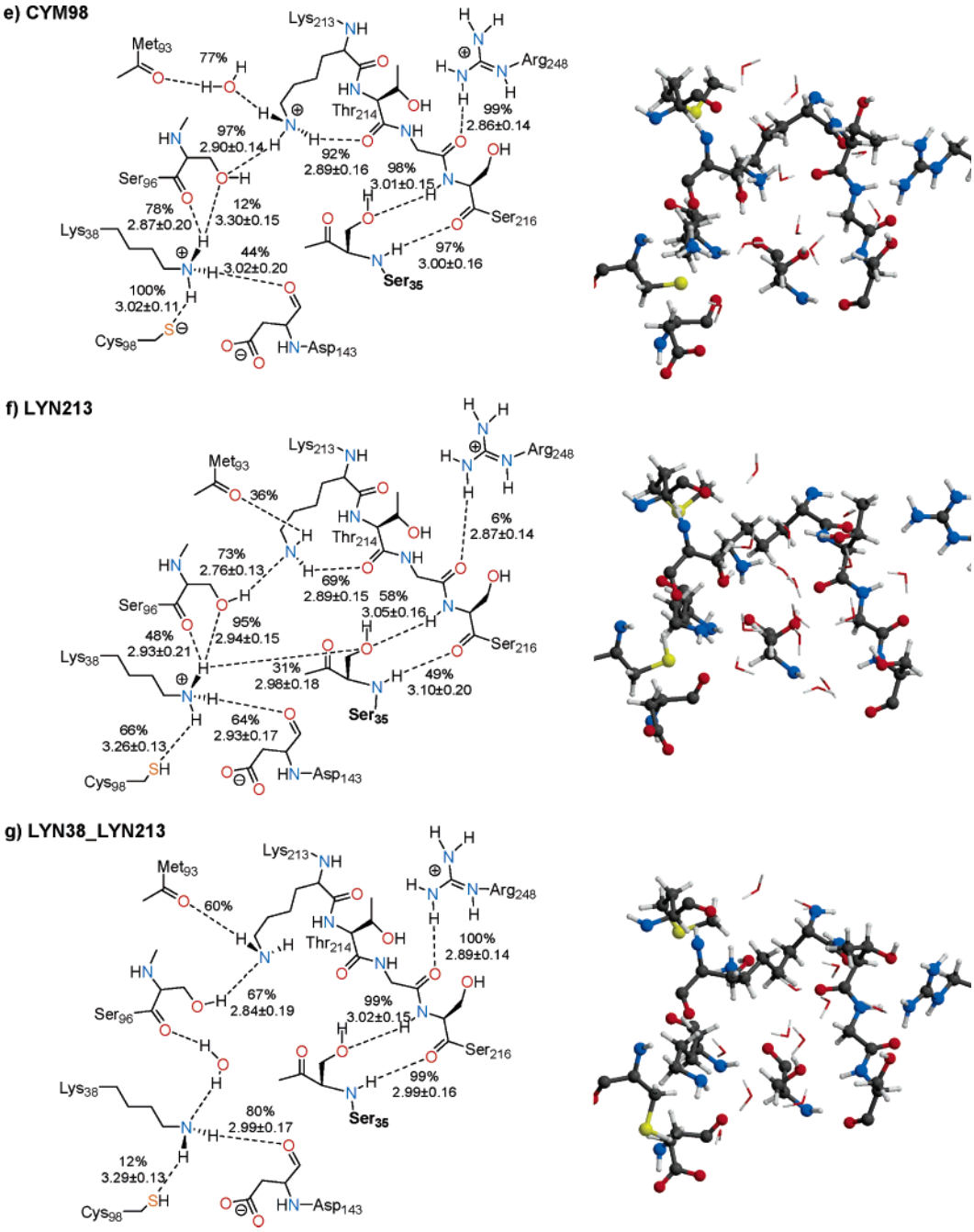

FIGURE 1: Schematic representation of the main interresidue contacts observed in the K15 PBP active site: (a) in the 1SKF X-ray structure and (b−g) along the six trajectories computed for the apo-enzyme. A snapshot of the active site extracted from each simulation has been produced with Molscript and Raster3D.

As mentioned above, all the apo-enzyme configurations have similar RMSD and RMSF values in aqueous solution. In addition, we see now that no single model can reproduce *all* the active site interresidue contacts observed in the solid state structure of the K15 enzyme. Therefore, it is not possible to characterize unambiguously the protonation state of the K15 active site on the basis of structural analyses. In this scenario, energetic calculations are clearly needed to estimate the relative stability of the different configurations studied for the K15 enzyme in aqueous solution.

QM Calculations on Small Cluster Models. The relative energetic stability of the K15 configurations is governed by several factors: (1) the intrinsic basicity of the Lys_{38}, Cys_{98}, Ser_{96}, and Lys_{213} side chains; (2) the strength of the hydrogen-bond network interconnecting the important residues in the active site; (3) protein−solvent interactions; (4) long-range protein−protein interactions. In principle, all these energetic contributions can be taken into account by means of semiempirical QM-PBSA calculations on protein subsystems. To calibrate the performance of the QM-PBSA approach as applied to our particular problem, we optimized a series of small cluster models in aqueous solution at the B3LYP/6-31G*, B3LYP/6-31+G**, and PM3 levels of theory. The corresponding energies and optimized geometries are reported in Table S3 and Figure S1 of the Supporting Information.

DFT optimizations of the small cluster models in solution led to stationary points that preserved the defining charge distribution and hydrogen-bonding network of the K15 configurations. In all these models, the heavy atom distance

between the thiol group and the ammonium/amine group at the Lys_{38} position lies between 3.2 and 4.2 Å, well above the 2.7 Å value of the original X-ray structure. The relative free energies in solution for the series of cluster models with a +1 charge, LYN38, SEN96, CYM98, and LYN213 are 0.0, +0.6, +7.7, and −0.6 kcal/mol, respectively, at the B3LYP/6-31+G** level. Numerical frequency calculations show that the small models LYN38, CYM98, and LYN213 correspond to stable minima on the PES, whereas the SEN96 model, which is characterized by short NH···O contacts (2.5−2.6 Å) of the methoxide group with the two nearby ammonium groups, turned out to be a transition structure for the assisted proton exchange between the Lys_{38} and Lys_{213} amino groups (see Figure S1, Supporting Information). This means that the SEN96 configuration of the small cluster model is not stable even in aqueous solution and that a low energy barrier of ∼1−2 kcal/mol separates the LYN38 and LYN213 configurations. On the other hand, we also estimated the relative stability of the LYN213 cluster model with respect to the LYS model by computing the free energy change in solution for the LYS → LYN213 + $H^+_{(aq)}$ process. We obtained a ΔG of +11.2 kcal/mol by combining the DFT free energies of the LYS and LYN213 models with experimental estimations of the proton thermodynamic data ($\Delta G_{solv}(H^+)$ = −259.5 kcal/mol; $T\Delta S$ = 7.9 kcal/mol at 298 K) previously used in QM pK_a calculations (*60*)).

The geometries and free energies of the small cluster models were computed using the semiempirical PM3 Hamiltonian as described above. The PM3 heavy atom distances in the N···O and N···S hydrogen-bond contacts are quite similar to the corresponding DFT values (see Figure S1). The relative semiempirical free energies for the LYN38, SEN96, CYM98, and LYN213 models (ΔG_{PM3}) are 0.0, 13.5, −7.3, and 1.2 kcal/mol, respectively. For the same cluster models, the corresponding free energy differences $\Delta G_{B3LYP/6-31+G^{**}} - \Delta G_{PM3}$ (0.0, −12.9, 15.0, and 1.8 kcal/mol) constitute the "high level correction" terms that can be applied to the QM-PBSA energies of the solvated protein subsystems. These correction factors indicate that PM3 slightly destabilizes the LYN213 configuration with respect to LYN38. The results for the CYM98 model, which is the most stable structure in solution at the PM3 level, shows that PM3 largely overestimates the acid strength of the thiol group by 15 kcal/mol as compared with the DFT results. Besides correcting the relative energy of the SEN96 configuration by around 13 kcal/mol, the DFT calculations introduce a qualitative change in the chemical significance of the SEN96 cluster model since the DFT structure, which has only a moderate ionic character, corresponds to a low barrier transition structure for the assisted proton exchange between the Lys_{38} and Lys_{213} amino groups. In contrast, the PM3 Hamiltonian characterizes the SEN96 configuration in solution as a strongly ionic structure corresponding to a high energy minimum on the PES. Similar observations have been reported in previous theoretical work (*61*) on model proton transfer reactions in symmetric hydrogen-bonded systems showing that PM3 tends to overestimate the energy barriers significantly (∼10 kcal/mol) with respect to ab initio results.

A good agreement between DFT and PM3 methodologies is found in the computation of the ΔG for the acid dissociation of the lysine ammonium groups. Thus, the semiempirical ΔG for the LYS → LYN213 + $H^+_{(aq)}$ process amounts to 10.8 kcal/mol (using the experimentally derived enthalpy of a proton; $\Delta H_f(H^+)$ = 365.7 kcal/mol (*62*)), which is very close to the DFT value (11.2 kcal/mol). We also note that semiempirical PM3 calculations for the butylammonium/butylamine pair (see Table 1) complemented with experimental thermodynamic data of $H^+_{(aq)}$ predict a pK_a value for *n*-butylamine of 11.0, which is very close to the experimental value (10.78). Hence, we did not derive a "high level correction" term for the acid dissociation processes.

Table 1: PM3-Based Free Energy Components[a] of the Different PBP K15 Configurations in Water[b]

system	H	ΔG_{solv}	G_{total}[c]
But-NH_2	−21.1 ± 0.9	−1.7 ± 0.2	−46.5 ± 0.9
But-NH_3^+	133.7 ± 0.6	−73.0 ± 1.3	36.8 ± 1.4
LYS	−2885.7 ± 45.2	−791.0 ± 30.8	−4440.0 ± 34.9
LYN38	−2960.5 ± 45.6 (0.0)	−805.6 ± 25.9 (0.0)	−4530.1 ± 39.8 (0.0)
SEN96	−2947.3 ± 40.9 (13)	−810.5 ± 26.7 (−5)	−4520.7 ± 31.6 (9)
CYM98	−2928.4 ± 37.8 (32)	−809.6 ± 21.7 (−4)	−4501.5 ± 31.0 (29)
LYN213	−2985.2 ± 42.9 (−25)	−794.7 ± 21.1 (11)	−4544.2 ± 42.9 (−14)
LYN38-LYN213	−3067.6 ± 38.9	−773.7 ± 26.9	−4605.5 ± 32.6

[a] In kilocalories per mole. [b] Relative differences of the SEN96, CYM98, and LYN213 mean values with respect to the LYN38 ones are in parentheses. Free energy components for the butylamine/butylammonium pair are also indicated. [c] Including the entropy corrections from MM normal mode calculations on subsystems.

Energetic Analyses of the MD Trajectories. The structure of the active site in selected snapshots along the MD trajectories was relaxed via QM/MM energy minimizations. In general, the QM/MM clusters, in which the Ser_{35}, Lys_{38}, Ser_{96}, Cys_{98}, Asp_{143}, Lys_{213}, and Thr_{214} residues were described by the PM3 method, were structurally similar to those generated along the MD simulations using the MM force field representation. For the CYM98 model, the average heavy atom Cys_{98}−S^-···^+H_3N-Lys_{38} distance in the PM3/AMBER minimized structures amounts to 2.95, which is still above the 2.7 Å value found in the X-ray crystal structure.

To assess the relative stability of the different models of the active site in solution, we performed single-point PM3 D&C-PB calculations and MM normal mode calculations on subsystems comprising ∼1/4 of the protein. These subsystems were built from the QM/MM relaxed structures along the MD trajectories as described in Methods. Table 1 shows the average heats of formation and solvation energies as estimated semiempirically. These values, which take into account the effects of the solvent continuum and the influence of structural fluctuations, can be combined with the MM entropy terms to obtain a first estimation of the free energy for each configuration (see Methods).

The average QM-PBSA free energy differences between the LYN213, SEN96, and CYM98 configurations and the LYN38 one are −14, 9, and 29 kcal/mol, respectively, thus favoring the neutral state of the Lys_{213} residue in the native form of the K15 enzyme (see Table 1). The magnitude of the estimated ΔG difference between CYM98 and LYN38 (+29 kcal/mol) suggests that the CYM98 state is indeed quite unstable in the protein. The semiempirical QM-PBSA calculations also suggest that the SEN96 configuration is less stable than the LYN38 and LYN213 states by 9 and 23 kcal/

mol, respectively. The energetic preference for the LYN213 state in the protein is not altered by adding the "high level corrections" as estimated by the DFT and PM3 calculations on the small cluster models. Thus, the corrected free energy differences of LYN213, SEN96, and CYM98 with respect to LYN38 are −16, −4, and +34 kcal/mol, respectively.

We also estimated the relative stability of the LYN213 configuration with respect to the LYS model in which both Lys_{38} and Lys_{213} are positively charged. We considered the free energy change for the proton dissociation process connecting formally the LYS and LYN213 states:

Scheme 2

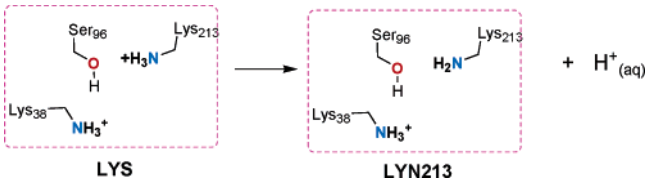

Combining the thermodynamic data for $H^+_{(aq)}$ with the *G* values for the LYS and LYN213 states in Table 1, the free energy change for the LYS → LYN213 + H^+ process amounts to −5.9 kcal/mol. Alternatively, we also considered the free energy change for a proton exchange process in solution as expressed by the following equation:

Scheme 3

The global free energy change for this process, which is obtained by subtracting the corresponding mean values in Table 1, is −20.9 kcal/mol, thus favoring the LYN213 + *n*-butylammonium state. Therefore, our calculations consistently predict that in solution the LYN213 configuration would be thermodynamically more stable than the LYS state regardless the reference reaction being analyzed. These results suggest that the *intrinsic* pK_a of the Lys_{213} group could be significantly lowered, resulting thus in a low value of its global pK_a.

In principle, the loss of a proton in the LYN38 or LYN213 configurations could formally lead to the LYN38_LYN213 state. To assess the stability of LYN38_LYN213 with respect to LYN213, we considered the free energy change associated to a formal process analogue to that in Scheme 3 (i.e., But-NH_2 + LYN213 → But-NH_3^+ + LYN38_LYN213). In this case, the corresponding Δ*G* obtained from the mean values collected in Table 1 is largely positive, +22 kcal/mol. Similarly, the Δ*G* value for the proton dissociation process LYN213 → L**Y**N38_LYN213 + H^+, 37 kcal/mol, is again very large and positive. Although other situations could be examined by means of these and other reference processes, it is likely that the LYN213 protonation state of the native enzyme would remain as the most favorable one in aqueous solution.

Structural Analyses of the K15−BP Complexes: RMSD and RMSF. The Michaelis complex formed between the K15 enzyme and benzylpenicillin was modeled in four different configurations of the active site (LYS−BP, LYN38−BP, SEN96−BP, and LYN213−BP) that corresponded to the energetically more favorable states of the free enzyme (LYS, LYN38, SEN96, and LYN213). Table S4 of the Supporting Information collects the RMSD and RMSF values for these configurations.

Comparison of the RMSD values in Table S4 with those in Table S1 shows that penicillin binding does not induce large changes in the global structure of the protein. Concerning the protein flexibility, the RMSF values for the four trajectories of the Michaelis complex are quite similar (0.8−1.0 Å). At the level of the active site residues, location of BP at the interface of the two domains of the enzyme reduces the active site flexibility in the LYN38−BP and LYN213−BP configurations, which could be an indication of better enzyme−ligand contacts along these trajectories (see below).

Interresidue Contacts in the K15−BP Complexes. Figure 2 shows schematic representations of the relevant hydrogen-bond contacts observed in the K15 active site and characteristic snapshots extracted from the MD trajectories in the presence of BP. Binding to BP induces some changes in the active site interresidue contacts with respect to those previously described for the apo-enzyme. For example, the nucleophilic hydroxyl group (Ser_{35}), which is replaced in the "oxy-anion hole" by the *β*-lactam carbonyl group, interacts directly with the Lys_{38} side chain along the four trajectories. The donor/acceptor nature of the Ser_{35}···Lys_{38} hydrogen-bond interaction depends on the protonation state of Lys_{38}. Thus, the LYN38−BP trajectory results in a stable Ser_{35}−O*γ*H···N*ζ*-Lys_{38} contact (2.77 ± 0.12Å, 100%), whereas the serine hydroxyl group behaves as an hydrogen-bond acceptor (Ser_{35}−O*γ*···HN*ζ*-Lys_{38}) in the LYS−BP, SEN96−BP, and LYN213−BP complexes (see Figure 2).

Other structural changes induced by inhibitor binding affect the Lys_{38}···Ser_{96}···Lys_{213} association. Thus, the Lys_{38}···Ser_{96} contact observed along the LYN38, SEN96, and LYN213 trajectories is lost in the LYN38−BP and LYN213−BP states (see Figure 2). The Lys_{38} side chain maintains a weak interaction with the thiol group of Cys_{98}, similar to that observed for the apo-enzyme, while the stability of its hydrogen bond with the Asp_{143} carbonyl group is reinforced by the presence of the antibiotic (except for the SEN96 configuration). It may be interesting to note that the salt bridge between the Lys_{38} and Asp_{143} observed along the LYS trajectory (2.78 ± 0.12 Å, 57%) becomes stabilized along the LYS−BP simulation (2.78 ± 0.12 Å, 88%). Similarly, the stability of the Arg_{248}−N*η*H···O-Gly_{215} contact is significantly increased in the LYN38−BP and LYN213−BP configurations. This contact is lost along the LYS−BP and SEN96−BP trajectories.

K15−BP Binding Determinants. The three structural parts of benzylpenicillin (i.e., the four-membered *β*-lactam ring, the five-membered thiazolidine ring, and the acylamino side chain) contribute to anchor the antibiotic to the K15 active site by means of specific interactions with residues of the enzyme. Our simulations show that the stability of the enzyme−inhibitor contacts in the Michaelis complexes and the relative orientation between the nucleophilic serine and the *β*-lactam cycle depend on the configuration of the active site residues. The relative orientation of the reactive groups together with the presence of long-lived contacts between the nucleophilic serine side chain and a potential base catalyst (the *β*-lactam carboxylate or the side chains of Lys_{38}, Ser_{96}, or Lys_{213}) allow us to assess the prereactive character of each configuration.

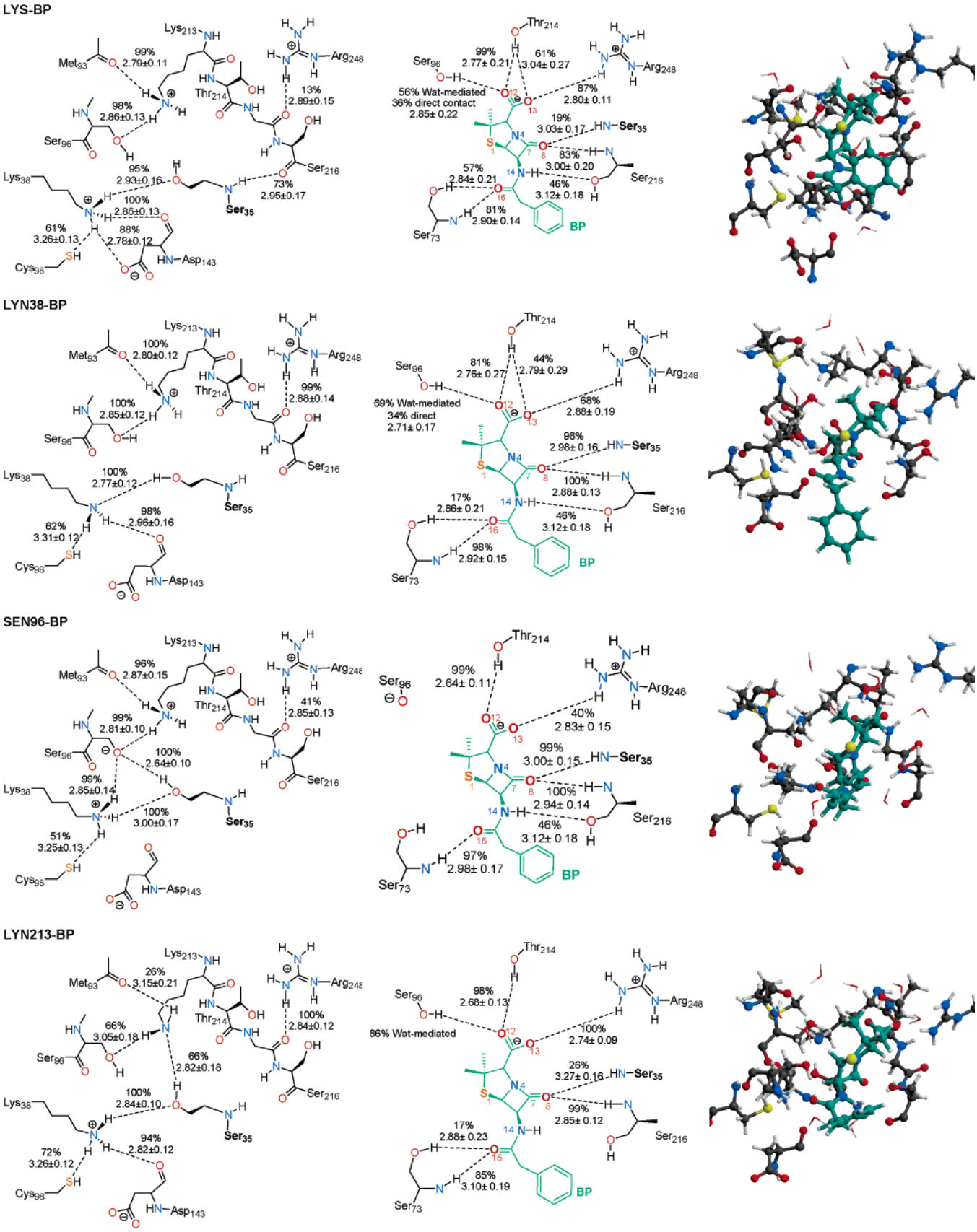

FIGURE 2: Schematic representation of the main interresidue contacts and enzyme−inhibitor binding determinants observed along the four trajectories computed for the Michaelis complex formed between benzylpenicillin and the K15 PBP enzyme. A snapshot of the active site extracted from each simulation with benzylpenicillin shown in green has been produced with Molscript and Raster3D.

Along the LYS−BP trajectory, the antibiotic molecule in the K15 active site shifts and changes its initial orientation with respect to the nucleophilic serine (Ser_{35}). On one hand, the β-lactam carbonyl moiety keeps its interaction with the backbone amino group of Ser_{216} (3.00 ± 0.20 Å, 83%), but the BP−O8···HN−Ser_{35} contact is lost after ~400 ps of

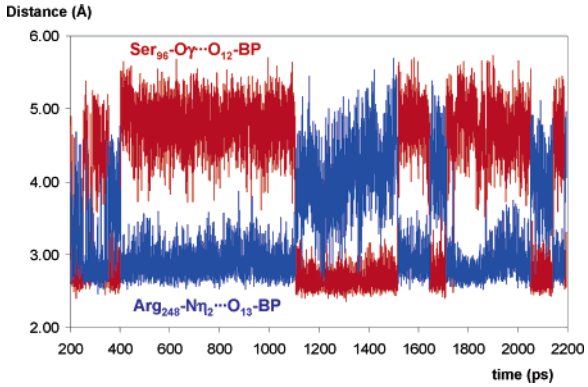

FIGURE 3: Time evolution of the Ser_{96}−Oγ···O12−BP (in red) and Arg_{248}−Nη2···O13−BP (in blue) distances along the LYN38−BP simulation.

simulation time so that the β-lactam carbonyl group is not properly placed at the "oxy-anion hole". On the other hand, the interaction between the BP carboxylate and the Arg_{248} side chain evolves from an initial Arg_{248}−NηH22···O13−BP hydrogen bond (2.77 ± 0.15 Å 10%) to the most abundant Arg_{248}−NηH21···O13−BP contact (2.80 ± 0.11 Å 87%). The BP−COO^- group also interacts with the side chains of Ser_{96} (36% of direct contacts and 56% of water-mediated interactions) and Thr_{214} (2.77 ± 0.21 Å, 99%). Finally, the carbonyl group of the acyl-amino side chain of BP interacts with the backbone amine group of Ser_{73} (Ser_{73}−NH···O16−BP 2.90 ± 0.14 Å, 81%).

In principle, the carboxylate moiety of benzylpenicillin is the only group capable of activating the Ser_{35} hydroxyl group in the LYS configuration. However, the BP−COO^- and Ser_{35}−OγH groups do not interact during the LYS−BP simulation either directly or through a water molecule. Moreover, the nucleophilic Ser_{35} side chain is nearly in a coplanar position with respect to the β-lactam ring (the average Ser_{35}−Oγ···O8−C7−N4−BP torsional angle is −162.7 ± 28.4°). In this orientation, the Ser_{35} side chain interacts with solvent molecules or with the carbonyl group of the acyl-amino side chain of BP (2.75 ± 0.17 Å, 18%). The average Ser_{35}−Oγ···C7−BP distance (4.20 ± 0.50 Å) and Ser_{35}−Cβ-Oγ···C7−BP angle (63.4 ± 17.9°) further demonstrates that the relative orientation of the Ser_{35} side chain and the β-lactam ring of BP is not adequate for the nucleophilic attack to occur. Thus, we conclude that BP adopts a nonreactive configuration in the K15 active site when both Lys_{38} and Lys_{213} are protonated, a result similar to that obtained in the previous MD simulation of the K15/cefoxitin Michaelis complex (*28*).

The LYN38−BP trajectory is characterized by stable Ser_{35}−NH···O8−BP (2.98 ± 0.16 Å, 98%) and Ser_{216}−NH···O8−BP (2.88 ± 0.13 Å, 100%) hydrogen-bond contacts, which maintain the β-lactam carbonyl group within the "oxy-anion hole". The "carboxylate pocket" constituted by the protein residues that interact with the BP carboxylate turns out to be quite flexible given that the BP−COO^- group oscillates between the Lys_{213} ammonium and the Arg_{248} guanidinium groups. In the most abundant complexes, the β-lactam carboxylate interacts directly with Arg_{248} (Nη2H···O13−BP = 2.88 ± 0.19 Å, 68%) and through a water molecule with the Ser_{96} side chain (69% of the simulation time). In the alternative conformation of the "carboxyate pocket", which was observed in 34% of the analyzed snapshots, the Arg_{248}−Nη2H···O13−BP hydrogen bond is not present, the bridging water molecule in Ser_{96}−OγH···OH_2···O12−BP has been expelled, and the Ser_{96} side chain mediates a salt bridge contact between the carboxylate moiety of BP and the ammonium group of Lys_{213} (Lys_{213}−NζH_3^+···Ser_{96}−OγH···O12−BP). Several transitions between these two binding modes of the BP−COO^- group occur during the course of the dynamics as shown in Figure 3, which represents the time evolution of the Ser_{96}−Oγ···O12−BP and Arg_{248}−Nη2···O13−BP distances. The shift of the BP carboxylate group between the positively charged side chains of Lys_{213} and Arg_{248} also perturbs its contact with the Thr_{214} side chain (see Figure 2) since interchangeable hydrogen-bond contacts are observed with both oxygen atoms of the carboxylate group. On the other hand, the carbonyl group of the acylamino side chain of the antibiotic mainly interacts with the backbone of Ser_{73} (Ser_{73}−NH···O16−BP 2.92 ± 0.15 Å, 92%) like in the LYS−BP state.

From a mechanistic point of view, the LYN38 configuration is characterized by the presence of a neutral lysine in the K15 active site (Lys_{38}), which could act as a base catalyst by activating the Ser_{35} hydroxyl group. The stability of the Ser_{35}−OγH···Nζ-Lys_{38} hydrogen-bond contact (2.77 ± 0.12 Å, 100%) along the LYN38−BP trajectory supports this hypothesis. Moreover, both the short Ser_{35}−Oγ···C7−BP distance (3.13 ± 0.17 Å) and the Ser_{35}−Cβ-Oγ···C7−BP angle (95.7 ± 7.4°) confirm that the Ser_{35} side chain is well positioned to attack the amide group of the β-lactam ring.

The SEN96−BP trajectory also shows stable contacts between the β-lactam carbonyl group and the "oxy-anion hole" (Ser_{35}−NH···O8−BP 3.00 ± 0.15 Å, 99% and Ser_{216}−NH···O8−BP 2.94 ± 0.14 Å, 100%). In this case, the BP carboxylate group interacts with the Thr_{214} hydroxyl group (2.64 ± 0.11 Å, 99%) and through water-mediated contacts with the Ser_{96} and Lys_{213} side chains (55 and 95%, respectively). In addition, there is a salt-bridge between the BP carboxylate and the Arg_{248} guanidinium groups either through a direct contact in the first half of the trajectory or through a water-mediated interaction in the second half. Again the C7 side chain of BP remains hydrogen bonded to Ser_{73} (Ser_{73}−NH···O16−BP 2.98 ± 0.17 Å, 97%).

The SEN96 configuration is characterized by the presence of the unusual anionic state of the Ser_{96} residue, which could be stabilized in the K15 active site by means of its ionic contacts with the Lys_{38} and Lys_{213} ammonium groups (see Figure 2). The anionic serine strongly interacts with the nucleophilic hydroxyl group (Ser_{35}−OγH···$^-$Oγ−Ser_{96} 2.64 ± 0.10Å, 100%), highlighting its potential catalytic relevance. Similarly, the average values of the Ser_{35}−Oγ···C7−BP distance (3.14 ± 0.16 Å) and the Ser_{35}−Cβ−Oγ···C7−BP angle (95.9 ± 8.1°) suggest that the Ser_{35} side chain is well positioned to attack the amide group of the β-lactam ring along the SEN96−BP trajectory.

The fourth simulation of the K15−BP Michaelis complex corresponds to the LYN213 configuration, which is the most probable state of the apo-enzyme according to our calculations. Along the LYN213−BP trajectory, the β-lactam carbonyl group partially occupies the "oxy-anion hole": the inhibitor carbonyl group keeps a stable hydrogen-bond contact with the amino group of Ser_{216} (2.85 ± 0.12 Å, 99%), but the orientation of the Ser_{35} side chain does not allow a proper Ser_{35}−NH···O8−BP interaction (3.27 ± 0.16 Å,

Table 2: PM3-Based Free Energy Components[a] of the PBP−K15 Enzyme Bound to Benzylpenicillin[b]

system	H	ΔG_{solv}	G_{total}[c]
LYS−BP	−3141.2 ± 38.2	−741.1 ± 24.5	−4673.8 ± 27.4
LYN38−BP	−3167.4 ± 29.4 (0.0)	−813.8 ± 15.9 (0.0)	−4773.4 ± 30.4 (0.0)
SEN96−BP	−3153.6 ± 32.6 (14)	−810.1 ± 21.0 (4)	−4753.0 ± 30.7 (20)
LYN213−BP	−3203.7 ± 33.6 (−36)	−762.8 ± 25.5 (51)	−4761.0 ± 36.5 (12)

[a] In kilocalories per mole. [b] Relative differences of the SEN96-BP, and LYN213-BP mean values with respect to the LYN38-BP ones are in parentheses. [c] Including the entropy corrections from MM normal mode calculations on subsystems.

26%). The BP−COO^- group establishes stable hydrogen bonds with Thr_{214} and Arg_{248} (see Figure 2) and is linked to Ser_{96} through a water bridge. The carbonyl group of the acylamino side chain of BP interacts with Ser_{73}, although this contact is weaker than those found in the other simulations (see Figure 2).

Along the LYN213−BP trajectory, the nucleophilic serine interacts with the neutral amino group of Lys_{213} through a Lys_{38}−NζH_3^+···Ser_{35}−OγH···H_2Nζ−Lys_{213} association. This could be indicative of a possible mechanistic role of the neutral Lys_{213} amino group as the base catalyst. However, the relatively large Ser_{35}−Oγ···C7−BP distance (4.29 ± 0.26 Å), the low value of the Ser_{35}−Cβ−Oγ···C7−BP angle (54.4 ± 10.6°), and the weak interaction of the β-lactam carbonyl group with the "oxy-anion hole", suggest that the LYN213−BP configuration should be less reactive than the LYN38−BP or SEN96−BP ones.

Energetic Analyses of the K15−BP Complexes. The thermodynamic analyses were repeated for the protein subsystems in the LYS−BP, LYN38−BP, SEN96−BP, and LYN213−BP trajectories following the QM-based computational scheme after having partially relaxed the selected snapshots by means of QM/MM energy minimizations. Examination of the average values of some QM/MM distances between the BP inhibitor and important residues in the K15 active site shows that the QM/MM relaxation does not alter the identity and properties of the important hydrogen-bond interactions that anchor the β-lactam to the K15 active site (data not shown for brevity).

Table 2 shows the average heats of formation, solvation energies, and free energies of the K15−BP complexes. Interestingly, the presence of the antibiotic reverses the energetic preference of the protein configuration given that the LYN38−BP state is now 12 and 20 kcal/mol below LYN213−BP and SEN96−BP, respectively, in terms of their mean semiempirical G values. Addition of the "high level correction" terms derived from the test calculations to the QM-PBSA G values preserves the energetic preference for the LYN38 state, which remains 10 and 7 kcal/mol below LYN213−BP and SEN96−BP, respectively.

To find out if the presence of the BP inhibitor can change the global charge distribution of the K15 active site by stabilizing energetically the LYS−BP complex with respect to LYN38−BP, we considered the formal proton dissociation process, LYS−BP → LYN38−BP + $H^+_{(aq)}$, which has a ΔG value of −1.3 kcal/mol as estimated semiempirically. Although this value is about 4 kcal/mol lower in absolute value than that for the LYS → LYN213 + $H^+_{(aq)}$ process in the absence of BP, it is still negative, suggesting thus that LYN38−BP would be the predominant configuration of the K15−BP complex in aqueous solution.

The QM-based binding energies ($\Delta G_{binding}$) are collected in Table 3 for the four K15−BP models. In the absence of the Lennard-Jones energy term, the absolute values of the $\Delta G_{binding}$ energies were largely positive (∼40−50 kcal/mol). In terms of their relative $\Delta G_{binding}$ energies, the LYS−BP (41.8 kcal/mol) and LYN38−BP (44.5 kcal/mol) models present a similar affinity for the BP inhibitor. In contrast, when the K15 enzyme is modeled in the LYN213 or SEN96 configurations, BP is a worse ligand by ∼13−15 kcal/mol. Inclusion of the attractive Lennard-Jones energy term to account for the dispersion interactions makes the $\Delta G_{binding}$ energies clearly negative (−20, −30 kcal/mol), showing thus the importance of the dispersion energy contribution to the total $\Delta G_{binding}$. Nevertheless, the observed trend in the relative $\Delta\Delta G_{binding}$ values remains unaltered (see Table 3). By examining the free energy components in Table 3, we see that the driving force for inhibitor binding in the LYS−BP state arises from intraprotein interactions between the negatively charged BP inhibitor and the K15 active site, which bears two ammonium groups at Lys_{38} and Lys_{213}. In the LYN38−BP complex, however, the inhibitor orientation and binding interactions result in a lower desolvation penalty, which compensates the weaker K15−BP interactions, leading to a relatively large value of $\Delta G_{binding}$.

DISCUSSION

The Native Form of the K15 Enzyme in Aqueous Solution. From the structural analyses of the MD trajectories corresponding to the unbound form of the K15 enzyme, it is not possible to determine the best theoretical model accounting for the structure of the K15 enzyme in the crystal state. Our energetic analyses predict that the LYN213 configuration is the most stable one in aqueous solution. The most significant structural features of the LYN213 trajectory are the ability of the Ser_{35} side chain to leave the "oxy-anion hole", and the presence of a Lys_{38}−N$_\zeta H_3^+$···Ser_{96}−O$_\gamma$H···:N$_\zeta H_2$−Lys_{213} hydrogen-bonding network. On one hand, the flexibility of the Ser_{35} side chain could facilitate the access to the "oxy-anion hole" of the carbonyl group of an incoming peptide substrate or β-lactam inhibitor. On the other hand, the stability of the Lys_{38}−NζH_3^+···Ser_{96}−OγH···:NζH_2-Lys_{213} association indicates that an hydrogen-shift process could take place between both lysine residues (see below). In this respect, the DFT calculations on the small cluster models suggest that the Ser_{96} hydroxyl group could be important in assisting the proposed proton-transfer process through a low barrier transition structure with an ionic structure Lys_{38}−NζH_3^+···Ser_{96}−Oγ^-···$^+H_3$Nζ-Lys_{213} resembling the SEN96 configuration. Nevertheless, the LYN213 → LYN38 conversion in the apo-enzyme would be disfavored according to free energy calculations.

The LYN213 model as the most stable enzyme configuration in solution is partly in consonance with previous electrostatic calculations that assigned a low pK_a (7.4) to Lys_{213} in the K15 enzyme (*28*). The same calculations also attributed a pK_a value of 7.2 to Cys_{98}, suggesting that this active site residue could be also deprotonated at the physi-

Table 3: Binding Free Energy Components[a] in the PBP−K15/β-Lactam Complexes as Obtained from the PM3-Based Energy Analyses without and with the Dispersion Energy Correction as Estimated by the AMBER Lennard-Jones Term[b]

	$\Delta H_{binding}$		$\Delta\Delta G_{solv}$	$\Delta G_{binding}$[c]	
		including LJ/R^6			including LJ/R^6
LYS−BP	−102.9 ± 9.2 (*0*)	−175.1 ± 14.4 (*0*)	125.2 ± 7.6 (*0*)	41.8 ± 10.5 (*0*)	−30.5 ± 15.9 (*0*)
LYN38−BP	−68.9 ± 7.8 (*34*)	−139.4 ± 10.1 (*36*)	92.7 ± 5.9 (*−32*)	44.5 ± 6.8 (*3*)	−26.0 ± 9.8 (*4*)
SEN96−BP	−47.7 ± 10.9 (*55*)	−108.5 ± 13.5 (*67*)	85.0 ± 6.6 (*−40*)	56.9 ± 9.6 (*15*)	−3.8 ± 12.4 (*27*)
LYN213−BP	−56.9 ± 7.8 (*46*)	−114.8 ± 9.0 (*60*)	94.2 ± 7.6 (*−31*)	54.7 ± 7.2 (*13*)	−3.2 ± 7.4 (*27*)

[a] In kilocalories per mole. [b] Relative differences with respect to the LYS−BP configuration are in parentheses. [c] Including the entropy corrections from MM normal mode calculations on subsystems. The standard state is to be taken 1 M.

ological pH. However, an anionic Cys_{98} side chain would be very unstable in the K15 active site according to our calculations. Similarly, previous mutagenesis experiments have not supported the presence of the anionic form of Cys_{98} (*25*). Furthermore, in the majority of the PBPs, the equivalent Cys_{98} residue corresponds to a neutral asparagine. We believe that the low pK_a value predicted for the Cys_{98} residue could be due to the short Lys_{38}−N$\zeta\cdots$Sγ−Cys_{98} distance observed in the X-ray structure, 2.7 Å, which seems clearly too low as revealed by our quantum chemical calculations at different levels of theory.

Binding of Penicillins to the K15 Active Site. By means of molecular modeling, docking analyses, and a short MD simulation with appropriate constraints, we built an initial structure for the complex formed between the K15 enzyme and benzylpenicillin in which the β-lactam carbonyl group interacts simultaneously with the two backbone NH groups of Ser_{35} and Ser_{216} (the "oxy-anion hole"), while the nucleophilic Oγ@Ser_{35} atom is well poised for attacking the β-lactam amide group. To the best of our knowledge, X-ray crystal structures of enzyme-ligand complexes for the K15 enzyme, which could have been used to inform the model building process, have not been reported. However, our docking calculations and MD simulations are in reasonable agreement with structural data available for other PBP/β-lactam covalent complexes (acyl-enzyme intermediates) involving PBP2x from *Streptococcus pneumoniae* (PDB code: 1QMF) (*63*), PBP2a from *Staphylococcus aureus* (1MWS, 1MWT, and 1MWU) (*64*), and the DD-carboxypeptidase from *Streptomyces R61* (1PW8, 1PWC, 1PWD, and 1PWG). The main enzyme-ligand contacts observed in all these structures are (1) the β-lactam carbonyl group located in the "oxy-anion hole"; (2) the β-lactam carboxylate group interacting with a hydroxyl group from strand β3; (3) the β-lactam acyl-amino side chain hydrogen bonded to an amino group of the enzyme.

The dynamic evolution of the initial K15−BP complex was explored by carrying out four 2-ns MD simulations differing in the charge configuration of the Lys_{38}, Ser_{96}, and Lys_{213} residues (LYS−BP, LYN38−BP, SEN96−BP, and LYN213−BP). Most interestingly, we found that the β-lactam carbonyl group remains properly located within the "oxy-anion hole" and has a short BP−C7$\cdots$Oγ−Ser_{35} distance (3.1 Å) during the LYN38−BP and SEN96−BP simulations, whereas the evolution of the LYS−BP and LYN213−BP models resulted in nonreactive and poorly reactive enzyme−inhibitor orientations, respectively (see Figure 2). On the other hand, free energy calculations and thermodynamic analyses predict that the LYN38−BP configuration is more stable than the SEN96−BP, LYN213−BP, and LYS−BP states. Therefore, we propose that upon formation of the K15−BP Michaelis complex the neutral form of Lys_{38} would become stabilized energetically to give a prereactive configuration.

From all discussed above, it is reasonable to expect that the Lys_{38}−NH_3^+/Lys_{213}−NH_2 pair characteristic of the LYN213 state, which is the most favored configuration of the apo-enzyme, would evolve into the Lys_{38}−NH_2/Lys_{213}−NH_3^+ pair when the BP antibiotic approaches the K15 active site. We expect that this process occurs easily in the K15 enzyme given that (a) the Lys_{38}/Lys_{213} ammonium/amino groups are bridged by the Ser_{96} hydroxyl group (in the LYN213 state) or the Ser_{35} hydroxyl group (in the LYN213−BP state); (b) abstraction of the hydroxyl proton by the Lys_{213} amino group to give a Lys_{38}−N$\zeta H_3^+\cdots$Ser−O$\gamma^-\cdots{}^+H_3$Nζ−Lys_{213} transition structure should not be energetically costly as suggested by the DFT calculations. Hence, the electrostatic influence of the negatively charged carboxylate group of BP, which points toward the Lys_{213} and Arg_{248} side chains, could promote the required Lys_{38}−NH_3^+ → Lys_{213}−NH_2 proton transfer at some stage during the approach of BP to the K15 active site.

We note in passing that previous electrostatic pK_a calculations for the K15 enzyme complexed with cefoxitin have predicted a high pK_a value for Lys_{38} (>14.0) in disagreement with our calculations (*28*). However, the pK_a calculations had been carried out using the coordinates of a single K15−cefoxitin complex generated by means of a rigid docking analysis.

Implications for the Acylation Mechanism of the K15 Enzyme. Binding of benzylpenicillin to the K15 active site would trigger the conversion from the LYN213 configuration of the apo-enzyme to the most reactive LYN38−BP complex. This process can be considered as the first step along the reaction mechanism for the formation of the K15 acyl-enzyme. As revealed by the LYN38−BP MD simulation, the β-lactam carbonyl group lies very close to the hydroxyl group of the nucleophilic Ser_{35} that in turn interacts with the neutral Lys_{38} amino group by means of a stable hydrogen bond. Hence, provided that the Ser_{35}−OγH proton is abstracted by the Lys_{38}−NζH_2 group, the nucleophilic attack could occur to give a tetrahedral intermediate (see Scheme 4). In this second step, the neutral Lys_{38} amino group would act as the base catalyst in agreement with the previous

Scheme 4

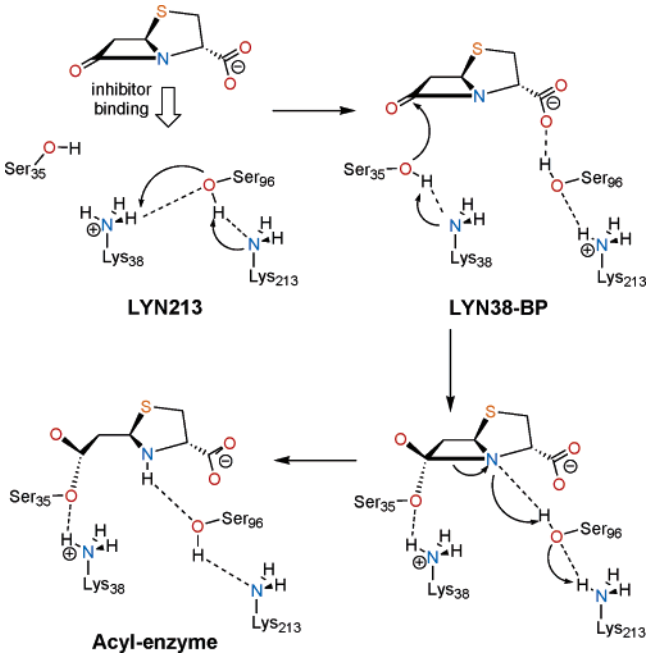

mechanistic proposals of Rhazi et al. based on their crystallographic, kinetic, and mutagenesis studies (*25*).

Subsequent protonation of the leaving amino group is required for the opening of the β-lactam ring of BP and the irreversible formation of the acyl-enzyme intermediate. This process is usually considered to occur with the assistance of a hydroxyl group conserved in the second structural motif of the active site (Ser_{96} in K15), which also constitutes one of the binding determinants of the carboxylate group of β-lactam antibiotics. On the basis of the stability of the $Ser_{96}-(O_\gamma H)\cdots{}^{+}H_3N_\zeta-Lys_{213}$ hydrogen-bond contact along the LYN38−BP simulation (2.85 ± 0.12 Å, 100%), we propose that the Lys_{213} ammonium group would be the required proton donor, while the Ser_{96} hydroxyl group would assist the proton transfer from Lys_{213} to the leaving amino group (see Scheme 4). At this point it may be interesting to note again that the BP carboxylate moiety gives flexible salt bridge interactions with the Lys_{213}/Arg_{248} ammonium/guanidinium groups throughout the LYN38−BP simulation. The moderate second-order rate constant experimentally observed for the acylation of the K15 enzyme by BP (150 M^{-1} s^{-1})(*26*) might be a consequence of the dynamical flexibility of the "carboxylate pocket" around the $BP-COO^-$ group as observed during the LYN38−BP simulation. The same dynamical effect might occur in the PBP5 enzyme from *Escherichia coli*, which has also an arginine residue (Arg_{198}) in its "carboxylate pocket" and a comparable rate constant for acylation by benzylpenicilin (390 M^{-1} s^{-1}) (*65*). In contrast, the PBP2x enzyme from penicillin-susceptible *Streptococcus pneumoniae*, which lacks a similar positively charged residue in its active site, is acylated more efficiently (200 000 M^{-1} s^{-1}) (*66*).

Finally, we comment on further mechanistic implications related to the presence of the *neutral* Lys_{213} amino group at the level of the acyl-enzyme intermediate. Thus, the $Lys_{213}-N\zeta H_2$ group might be properly positioned for activating a water molecule to give the (slow) hydrolysis of the acyl-enzyme intermediate that has been detected experimentally ($k_{hydrolysis} = 10^{-4}$ s^{-1}) (*26*). Similarly, the neutral Lys_{213} could activate the amino group of the peptide acceptor during the transpeptidization reaction of the peptidoglycan. Moreover, the uncharged Lys_{213} side chain in the acyl-enzyme form could be related to the behavior of the K15 enzyme as an strict DD-transpeptidase (in the absence of a peptide acceptor chain, the enzyme reutilizes the released D-Ala fragment as an acceptor to catalyze a silent reaction, that is, no carboxypeptidase activity is observed (*67*)). Given that the Arg_{248} side chain is able to interact with the BP-carboxylate group, particularly in the LYN213−BP state, it is conceivable that this residue could retain a leaving D-Ala fragment by giving a salt bridge interaction with the D-Ala carboxylate group. The neutral Lys_{213} could then activate the D-Ala amino group to attack the K15 acyl-enzyme and give globally a silent transpeptidization.

ACKNOWLEDGMENT

The authors are grateful to the CICyT (Spain) for allocation of computer time at the CESCA and the CIEMAT.

SUPPORTING INFORMATION AVAILABLE

Tables S1−S5 and Figure S1. This material is available free of charge via the Internet at http://pubs.acs.org.

REFERENCES

1. Coulson, C. J. (1995) *Molecular Mechanisms of Drug Action*, Taylor & Francis, London.
2. Tipper, D. J., and Strominger, J. L. (1965) Mechanism of action of penicillins: A proposal based on their structural similarity to acyl-D-alanyl-D-alanine, *Proc. Natl. Acad. Sci. U.S.A. 54*, 1133−1141.
3. Frère, J. M., Nguyen-Distèche, M., Coyette, J., and Joris, B. (1992) in *The Chemistry of Beta-Lactams* (Page, M. I., Ed.) pp 148−197, Blackie Academic & Professional, London.
4. Frère, J. M. (1995) Beta-lactamases and bacterial resistance to antibiotics, *Mol. Microbiol. 16*, 385−395.
5. Christensen, H., Martin, M. T., and Waley, S. G. (1990) Beta-lactamases as fully efficient enzymes, *Biochem. J. 266*, 853−861.
6. Waley, S. G. (1992) in *The Chemistry of Beta-Lactams* (Page, M. I., Ed.) pp 199−227, Blackie Academic & Professional, London.
7. Massova, I., and Mobashery, S. (1998) Kinship and diversification of bacterial penicillin-binding proteins and beta-lactamases, *Antimicrob. Agents Chemother*. 1−17.
8. Kelly, J. A., Kuzin, A. P., Charlier, P., and Fonzé, E. (1998) X-ray studies of enzymes that interact with penicillins, *Cell. Mol. Life Sci. 54*, 353−358.
9. Matagne, A., Lamotte-Brasseur, J., and Frère, J. M. (1998) Catalytic properties of class A beta-lactamases: Eficiency and diversity, *Biochem. J. 330*, 581−598.
10. Díaz, N., Sordo, T. L., Merz, K. M., Jr., and Suárez, D. (2003) Insights into the acylation mechanism of class A beta-lactamases from molecular dynamics simulations of the TEM-1 enzyme complexed with benzylpenicillin, *J. Am. Chem. Soc. 125*, 672−684.
11. Minasov, G., Wang, X., and Shoichet, B. (2002) An ultrahigh-resolution structure of TEM-1 beta-lactamase suggests a role for Glu166 as the general base in acylation, *J. Am. Chem. Soc. 124*, 5333−5340.
12. Strynadka, N. C. J., Adachi, H., Jensen, S. E., Johns, K., Sielecki, A., Betzel, C., Sutoh, K., and James, M. N. G. (1992) Molecular structure of the acyl-enzyme intermediate in β-lactam hydrolysis at 1.7 Å resolution, *Nature 359*, 700−705.
13. Maveyraud, L., Massova, I., Birck, C., Miyashita, K., Samama, J. P., and Mobashery, S. (1996) Crystal structure of 6α-(hydroxymethyl)penicillanate complexed to the TEM-1 β-lactamase from *Escherichia coli*: Evidence on the mechanism of action of a novel inhibitor designed by a computer-aided process, *J. Am. Chem. Soc. 118*, 7435−7440.

14. Chen, C. C. H., and Herzberg, O. (2001) Structures of the acyl-enzyme complexes of the *Staphylococcus aureus* beta-lactamase mutant Glu166Asp:Asn170Gln with benzylpenicillin and cephaloridine, *Biochemistry 40*, 2351−2358.
15. Guillaume, G., Vanhove, M., Lamotte-Brasseur, J., Ledent, P., Jamin, M., Joris, B., and Frère, J. M. (1997) Site-directed mutagenesis of glutamate 166 in two beta-lactamases, *J. Biol. Chem. 272*, 5438−5444.
16. Oefner, C., D'Arcy, D., Daly, J. J., Gubernator, K., Charnas, R. L., Heinze, I., Hubschwerlen, C., and Winkler, F. K. (1990) Refined crystal structure of beta-lactamase from *Citrobacter freundii* indicates a mechanism for beta-lactam hydrolysis, *Nature 343*, 284−288.
17. Dubus, A., Normark, S., Kania, M., and Page, M. G. (1994) The role of tyrosine 150 in catalysis of beta-lactam hydrolysis by AmpC beta-lactamase from *Escherichia coli* investigated by site-directed mutagenesis, *Biochemistry 33*, 8577−8586.
18. Lamotte-Brasseur, J., Dubus, A., and Wade, R. C. (2000) pK_a calculations for class C beta-lactamases: The role of Tyr-150, *Proteins 40*, 23−28.
19. Lee, W., McDonough, M. A., Kotra, L. P., Li, Z.-H., Silvaggi, N. R., Takeda, Y., Kelly, J. A., and Mobashery, S. (2001) A 1.2 Å snapshot of the final step of bacterial cell wall biosynthesis, *Proc. Natl. Acad. Sci. U.S.A. 98*, 1427−1431.
20. Silvaggi, N. R., Anderson, J. W., Brinsmade, S. R., Pratt, R. F., and Kelly, J. A. (2003) The crystal structure of phosphonate-inhibited D-Ala-D-Ala peptidase reveals an analogue of a tetrahedral transition state, *Biochemistry 42*, 1199−1208.
21. Gherman, B. F., Goldberg, S. D., Cornish, V. W., and Friesner, R. A. (2004) Mixed quantum mechanical/molecular mechanical study of the deacylation reaction in a penicillin binding protein versus in a class C beta-lactamase, *J. Am. Chem. Soc. 126*, 7652−7654.
22. Golemi, D., Maveyraud, L., Vakulenko, S., Samama, J. P., and Mobashery, S. (2001) Critical involvement of a carbamylated lysine in the catalytic function of class D beta-lactamases, *Proc. Natl. Acad. Sci. U.S.A. 98*, 14280−14285.
23. Davies, C., White, S. W., and Nicholas, R. A. (2001) Crystal structure of a deacylation-defective mutant of penicillin-binding protein 5 at 2.3 Å resolution, *J. Biol. Chem. 276*, 616−623.
24. Thomas, B., Wang, Y., and Stein, R. L. (2001) Kinetic and mechanistic studies of penicillin-binding protein 2x from *Streptococcus pneumoniae*, *Biochemistry 40*, 15811−15823.
25. Rhazi, N., Charlier, P., Dehareng, D., Engher, D., Vermeire, M., Frère, J.-M., Nguyen-Distèche, M., and Fonzé, E. (2003) Catalytic mechanism of the *Streptomyces* K15 DD-transpeptidase/penicillin-binding protein probed by site-directed mutagenesis and structural analysis, *Biochemistry 42*, 2895−2906.
26. Leyh-Bouille, M., Nguyen-Distèche, M., Pirlot, S., Vaithen, A., Bourguignon, C., and Ghuysen, J.-M. (1986) *Streptomyces* K15 DD-peptidase-catalysed reactions with suicide beta-lactam carbonyl donors, *Biochem. J. 235*, 177−182.
27. Fonzé, E., Vermeire, M., Nguyen-Distèche, M., Brasseur, R., and Charlier, P. (1999) The crystal structure of a penicilloyl-serine transferase of intermediate penicillin sensitivity, *J. Biol. Chem. 274*, 21853−21860.
28. Oliva, M., Dideberg, O., and Field, M. J. (2003) Understanding the acylation mechanisms of active-site serine penicillin-recognizing proteins: A molecular dynamics simulation study, *Proteins: Struct. Funct. Genet. 52*, 88−100.
29. Jorgensen, W. L., Chandrasekhar, J., Madura, J., Impey, R. W., and Klein, M. L. (1983) Comparison of simple potential functions for the simulation of liquid water, *J. Chem. Phys. 79*, 926−935.
30. Schafmeister, C., Ross, W. S., and Romanovski, V. (1995) *LEaP*, University of California, San Francisco.
31. Cornell, W. D., Cieplak, P., Bayly, C. I., Gould, I. R., Merz, K. M., Jr., Ferguson, D. M., Spellmeyer, D. C., Fox, T., Caldwell, J. W., and Kollman, P. A. (1995) A second generation force field for the simulation of proteins, nucleic acids, and organic molecules, *J. Am. Chem. Soc. 117*, 5179−5197.
32. Case, D. A., Pearlman, D. A., Caldwell, J. W., Cheatham, T. E., II, Ross, W. S., Simmerling, C. L., Darden, T. A., Merz, K. M., Jr., Stanton, R. V., Cheng, A. L., Vincent, J. J., Crowley, M., Ferguson, D. M., Radmer, R. J., Seibel, G. L., Singh, U. C., Weiner, P. K., and Kollman, P. A. (2002) *AMBER 7.0*, University of California, San Francisco.
33. Berendsen, H. J. C., Potsma, J. P. M., van Gunsteren, W. F., DiNola, A. D., and Haak, J. R. (1984) Molecular dynamics with coupling to and external bath, *J. Chem. Phys. 81*, 3684−3690.
34. Essman, V., Perera, L., Berkowitz, M. L., Darden, T., Lee, H., and Pedersen, L. G. (1995) A smooth particle-mesh-ewald method, *J. Chem. Phys. 103*, 8577−8593.
35. Kraulis, P. J. (1991) Molscript: A program to produce both detailed and schematic plots of protein structures, *J. Appl. Crystallogr. 24*, 946−950.
36. Merritt, E. A., and Bacon, D. J. (1997) Raster3d: Photorealistic molecular graphics, *Methods Enzymol. 277*, 505−524.
37. Morris, G. M., Goodsell, D. S., Halliday, R. S., Huey, R., Hart, W. E., Belew, R. K., and Olson, A. J. (1998) Automated docking using a lamarckian genetic algorithm and empirical binding free energy function., *J. Comput. Chem. 19*, 1639−1662.
38. Goodsell, D. S., and Olson, A. J. (1990) Automated docking of substrates to proteins by simulated annealing, *Proteins: Struct. Funct. Genet. 8*, 195−202.
39. Díaz, N., Sordo, T. L., and Suárez, D. (2003) Conformational properties of penicillins: Quantum chemical calculations and molecular dynamics simulations of benzylpenicillin, *J. Comput. Chem. 24*, 1864−1873.
40. Becke, A. D. (1995) in *Modern Electronic Structure Theory, Part II* (Yarkony, D. R., Ed.) World Scientific, Singapore.
41. *JAGUAR*, Schrödinger Inc., Portland, OR, 1991−2003.
42. Tannor, D. J., Marten, B., Murphy, R., Friesner, R. A., Sitkoff, D., Nicholls, A., Ringnalda, M., Goddard, I., W. A., and Honig, B. (1994) Accurate first principles calculation of molecular charge distributions and solvation energies from ab initio quantum mechanics and continuum dielectric theory., *J. Am. Chem. Soc. 116*, 11875−11882.
43. Stewart, J. J. P. (1989) Optimization of parameters for semiempirical methods. I. Method, *J. Comput. Chem. 10*, 209−220.
44. Gogonea, V., and Merz, K. M., Jr. (1999) Fully quantum mechanical description of proteins in solution. Combining linear scaling quantum mechanical methodologies with the Poisson-Boltzmann equation, *J. Phys. Chem. A 103*, 5171−5178.
45. Cheng, A., Stanton, R. S., Vincent, J. J., van der Vaart, A., Damodaran, K. V., Dixon, S. L., Hartsough, D. S., Mori, M., Best, S. A., Monard, G., Garcia, M., Van Zant, L. C., and Merz, K. M. J. (1999) *ROAR 2.0*, The Pennsylvania State University.
46. Baginski, M., Fogolari, F., and Briggs, J. M. (1997) Electrostatic and non-electrostatic contributions to the binding free energies of anthracycline antibiotics to DNA, *J. Mol. Biol. 274*, 253−267.
47. Kollman, P. A., Massova, I., Reyes, C., Kuhn, B., Huo, S., Chong, L., Lee, M., Lee, T., Duan, Y., Wang, W., Donini, O., Cieplak, P., Srinivasan, J., Case, D. A., and Cheatham, T. E. (2000) Calculating structures and free energies of complex molecules: Combining molecular mechanics and continuum models, *Acc. Chem. Res. 33*, 889−897.
48. Gohlke, H., and Case, D. A. (2003) Converging free energy estimates: MM-PB(GB)SA studies on the protein-protein complex ras−raf, *J. Comput. Chem. 25*, 238−250.
49. Goedecker, S. (1999) Linear scaling electronic structure methods, *Rev. Mod. Phys. 71*, 1085−1123.
50. Yang, W., and Lee, T.-S. (1995) A density-matrix form of the divide-and-conquer approach for electronic structure calculations of large molecules, *J. Chem. Phys. 103*, 5674−5678.
51. Dixon, S. L., and Merz, K. M., Jr. (1997) Fast, accurate semiempirical molecular orbital calculations for macromolecules, *J. Chem. Phys. 107*, 879−893.
52. Zheng, Y. J., and Merz, K. M., Jr. (1992) Study of hydrogen bonding interactions relevant to biomolecular structure and function, *J. Comput. Chem. 13*, 1161−1169.
53. Li, J., Cramer, C. J., and Truhlar, D. G. (1998) New class IV charge model for extracting accurate partial charges from wave functions, *J. Phys. Chem. A. 102*, 1820−1831.
54. Rappé, A. K., Casewit, C. J., Colwell, K. S., Goddard, W. A., III, and Skiff, W. M. (1992) Uff, a full periodic table force field for molecular mechanics and molecular dynamics simulations, *J. Am. Chem. Soc. 114*, 10024−10035.
55. Dixon, S. L., van der Vaart, A., Gogonea, V., Vincent, J. J., Brothers, E. N., Suárez, D., Westerhoff, L. M., and Merz, K. M. J. (1999) *DivCon99*, The Pennsylvania State University.
56. van der Vaart, A., Suárez, D., and Merz, K. M., Jr. (2000) Critical assessment of the performance of the semiempirical divide and conquer method for single point calculations and geometry optimizations of large chemical systems, *J. Chem. Phys. 113*, 10512−10523.
57. Lui, D. C., and Nocedal, J. (1989) On the limited memory BFGS method for large scale optimization, *Math. Programming 45*, 503−528.

58. Chong, L. T., Duan, Y., Wang, L., Massova, I., and Kollman, P. A. (1999) Molecular dynamics and free energy calculations applied to affinity maturation in antibody 48G7, *Proc. Natl. Acad. Sci. 96*, 14330−14335.
59. Raha, K., and Merz, K. M., Jr. (2004) A quantum mechanics-based scoring function: Study of zinc ion-mediated ligand binding, *J. Am. Chem. Soc. 126*, 1020−1021.
60. Cross, J. B., Duca, J. S., Kaminski, J. J., and Madison, V. J. (2002) The active site of a zinc-dependent metalloproteinase influences the computed pK_a of ligands coordinated to the catalytic zinc ion, *J. Am. Chem. Soc. 124*, 11004−11007.
61. Kallies, B., and Mitzner, R. (1995) The ability of the semiempirical PM3 method to model proton-transfer reactions in symmetric hydrogen bonded systems, *J. Mol. Model. 1*, 68−78.
62. Dewar, M. J. S., and Dieter, K. M. (1986), *J. Am. Chem. Soc. 108*, 8075−8086.
63. Gordon, E., Mouz, N., Duée, E., and Dideberg, O. (2000) The crystal structure of the penicillin-binding protein 2x from *Streptococcus pneumoniae* and its acyl-enzyme form: Implication in drug resistance, *J. Mol. Biol. 299*, 477−485.
64. Lim, D., and Strynadka, N. C. (2002) Structural basis for the beta-lactam resistance of pbp2a from methicillin-resistant *Staphylococcus aureus*, *Nat. Struct. Biol. 9*, 870−876.
65. Nicholas, R. A., Krings, S., Tomberg, J., Nicola, G., and Davies, C. (2003) Crystal structure of wild-type penicillin-binding protein 5 from *Escherichia coli*, *J. Biol. Chem. 278*, 52826−52833.
66. Lu, W.-P., Kincaid, E., Sun, Y., and Bauer, M. D. (2001) Kinetics of beta-lactam interactions with penicillin-susceptible and -resistant penicillin-binding protein 2x proteins from *Streptococcus pneumoniae*, *J. Biol. Chem. 276*, 31494−31501.
67. Nguyen-Distèche, M., Leyh-Bouille, M., Pirlot, S., Frère, J.-M., and Ghuysen, J.-M. (1986) *Streptomyces* K15 DD-peptidase-catalysed reactions with ester and amide carbonyl donors, *Biochem. J. 235*, 167−176.

BI048193G